J Mater Sci (2009) 44:4557–4571
DOI 10.1007/s10853-009-3691-5

Effect of pre- and post-weld heat treatment on metallurgical and tensile properties of Inconel 718 alloy butt joints welded using 4 kW Nd:YAG laser

X. Cao · B. Rivaux · M. Jahazi · J. Cuddy · A. Birur

Received: 25 November 2008 / Accepted: 15 June 2009 / Published online: 2 July 2009

Abstract The effects of pre- and post-weld heat treatments on the butt joint quality of 3.18-mm thick Inconel 718 alloy were studied using a 4 kW continuous wave Nd:YAG laser system and 0.89-mm filler wire with the composition of the parent metal. Two pre-weld conditions, i.e., solution treated, or solution treated and aged, were investigated. The welds were then characterized in the as-welded condition and after two post-weld heat treatments: (i) aged, or (ii) solution treated and aged. The welding quality was evaluated in terms of joint geometries, defects, microstructure, hardness, and tensile properties. HAZ liquation cracking is frequently observed in the laser welded Inconel 718 alloy. Inconel 718 alloy can be welded in pre-weld solution treated, or solution treated and aged conditions using high power Nd:YAG laser. Post-weld aging treatment is enough to strengthen the welds and thus post-weld solution treatment is not necessary for strength recovery.

X. Cao (✉) · B. Rivaux · M. Jahazi
Aerospace Manufacturing Technology Center, Institute for Aerospace Research, National Research Council Canada, 5145 Decelles Avenue, Montreal, QC H3T 2B2, Canada
e-mail: Xinjin.Cao@cnrc-nrc.gc.ca

B. Rivaux
Ecole des Mines de Paris, CEMEF – Materials Processing Center, Rue Claude Daunesse, BP 207, 06904 Sophia-Antipolis Cedex, France

J. Cuddy · A. Birur
Standard Aero Limited, 33 Allen Dyne Road, Winnipeg, MB R3H 1A1, Canada

Introduction

Inconel 718 is a precipitation-hardenable nickel–iron base superalloy widely used in gas turbines, rocket motors, spacecraft, nuclear reactors, pumps, and tooling due to its excellent combination of corrosion resistance, oxidation resistance, and good tensile and creep properties at temperatures up to 650 °C [1]. The strengthening is mainly produced by lens-like disc shaped γ''-Ni_3Nb coherent precipitates, with ordered bct DO22 crystal structure, and cubic or spherical shaped γ'-$Ni_3(TiAl)$ coherent precipitates, with ordered fcc LI2 crystal structure [2]. Niobium is the key alloying element and performs the strengthening role in both the γ'' and γ' phases for Inconel 718 alloy. However, the principal strengthening phase, γ'', is metastable and can be transformed to detrimental δ-Ni_3Nb when exposed at temperatures above 650 °C [2]. Prior to the introduction of Inconel 718 alloy in 1959, the precipitation-hardened nickel alloys, which were strengthened by either Al and/or Ti compounds underwent a rapid precipitation of the hardening phase during exposure to intermediate temperature range [3]. This rapid reaction caused difficulties in carrying out welding and repair without weld- or post-weld heat treatment associated cracking, which has been frequently encountered in the age-hardenable superalloys such as Waspaloy, Rene 41, Inconel X750, and Udimet 700. The Nb-containing 718 alloy has low Al and/or Ti contents. The introduction of niobium as the primary hardening element in Inconel 718 alloy resulted in a sluggish precipitating reaction of the principal strengthening precipitate γ'' phase, and produced a relatively low-strength, high ductility heat-affected zone during the initial aging treatment. This allowed more time for the alloy to achieve the desired hardness level and enabled stress to be relieved or relaxed before hardening. The improvement in

the strain-age cracking resistance and subsequently the prevention of strain-age cracking during post-weld heat treatment (PWHT) drastically improved weldability and repairability of nickel alloys [3, 4]. Strain-age cracking is also termed solid-state cracking, or PWHT stress relaxation cracking. Strain-age cracking usually occurs after welding or during precipitation-hardening heat treatment when the combination of stresses exceeds the material strength. The stresses include the residual welding stresses and those associated with precipitation reactions and fabrication processes.

Inconel 718 alloy has excellent weldability largely because of its resistance to strain-age cracking and reasonably good resistance to solidification cracking. Tungsten inert gas (TIG), electron beam (EB), and plasma welding techniques have been most widely used for precipitation-hardened nickel alloys [5, 6]. One of the major problems associated with the Inconel 718 alloy welding is microfissuring in the HAZ [1]. The HAZ liquation cracks (microfissures) have been frequently observed due to the interaction between grain boundary liquation and tensile stress. The microfissures usually occur under the nail head and are perpendicular to the fusion boundary. Another root concern for Inconel 718 alloy is the segregation of the element Nb and the consequent formation of the Nb-rich Laves phase, a brittle intermetallic compound represented as $(Ni, Cr, Fe)_2$ (Nb, Mo, Ti), in the interdendritic regions during weld metal solidification. Studies have shown that the formation of the Laves phase (i) depletes principal alloying elements required for hardening from the matrix, (ii) represents a weak-zone microstructure between the Laves phase and the matrix interface, (iii) acts as preferential sites for easy crack initiation and propagation because of its inherent brittle nature, and (iv) deteriorates the mechanical properties, especially tensile ductility, fracture toughness, fatigue, and creep rupture properties [7–9]. Because the formation of Laves phase is due to segregation during weld solidification, any effort to minimize the formation of Laves phase should be directed towards minimizing the segregation. This is well-achieved using a low heat input or high cooling rate welding process such as laser beam technique. High energy density laser beam is characterized with high welding speed, flexibility, and ease of automation. Moreover, its low overall heat input also produces low distortion and minimizes the width of the fusion zone and the HAZ [1]. Therefore, laser welding is very attractive for Inconel 718 alloy. It has been reported that microfissures can even be avoided using a low power pulsing wave Nd:YAG laser [4, 7, 10] and high power CO_2 laser [5].

To date, little work has been carried out using a high power continuous wave solid-state Nd:YAG laser for Inconel 18 alloy welding. It is interesting to investigate whether the HAZ microfissuring is still an issue for Inconel 718 alloy welded using a high power continuous wave solid-state Nd:YAG laser. It is usually advised that (i) precipitation-hardened nickel alloys should be welded in the solution treated state, and (ii) post-weld solution and aging treatments should be carried out for precipitation hardening [6]. Some interesting topics are therefore to investigate whether a high power Nd:YAG laser can be used to reduce the full post-weld heat treatment to aging only or to weld the materials directly in the solution and aged state. Hence, investigation into the effects of heat treatment conditions prior to and after welding on joint quality is essential. In this study, a 4 kW continuous wave Nd:YAG laser system was used to weld 3.18-mm thick Inconel 718 alloy butt joints and the influence of pre- and post-weld heat treatment conditions on welding quality is investigated in terms of weld defects, microstructure, hardness, and tensile properties.

Experimental procedures

The experimental material used in this article is Inconel 718 alloy with a nominal thickness of 3.18 mm in two pre-weld heat treatment conditions: (i) solution treated (STed) in the as-received material form (980 °C for 1 h and air cooled), and (ii) solution treated and aged (STAed). Solution treating is a high-temperature heat treatment designed to put age-hardening constituents and carbides into solid solution, i.e., solubilizing the Nb-rich Laves phase and producing a homogenized microstructure. The latter is generally obtained only through aging treatment of the as-received material in solution treated condition. The aging consisted of the following steps: solution at 718 °C for 8 h, furnace cool to 621 °C in 2 h, hold at 621 °C for 8 h, and argon quench. The room temperature tensile properties of the 3.18-mm thick Inconel 718 alloy sheets in the roll direction in both the solution treated (STed) and the solution treated and aged (STAed) conditions are indicated in Table 1. The alloy sheet was sheared into 102 × 63 × 3.18 mm coupons with the longitudinal direction (welding direction) normal to the rolling direction. The surface oxides were then removed and cleaned with ethanol prior to laser welding.

Table 1 Mechanical properties of 3.18-mm Inconel 718 base alloy sheets

	Solution treated	Solution treated and aged
Yield strength 0.2% (MPa)	470	1209
Tensile strength (MPa)	887	1398
Elongation (%) at 50-mm gage length	48.8	21.4
Hardness (HV)	210	440

The coupons were clamped using bolts in a restraint fixture designed for a butt joint configuration. The fixture was placed on the electromagnetic table of the laser welding system. The welding machine was a continuous wave solid-state 4 kW Nd:YAG laser system equipped with fiber optic beam transmission and an ABB 4400 industrial robot. In this study, all laser welding experiments were performed using the optimized processing parameters obtained in an earlier work [11] where the effect of joint gap ranging from zero (no gap) to 0.5 mm on the quality of Inconel 718 alloy butt joints was investigated using 0.89 mm (0.035″) filler wire with the composition of the parent material. Inconel 718 alloy is usually laser welded autogenously but the use of filler wire can lower the sensitivity to joint gaps, eliminate underfill, and undercut defects, and hence improve welding process. These optimized parameters used in this work are 0.3-mm joint gap, 3.0-m/min welding speed, and 4-kW laser power. To prevent oxidation during welding, argon (at a flow rate of 23.6 L/min) was applied to the top and helium (47.2 L/min) to the tail and the bottom surfaces of the joint. The defocusing distance used is −1.0 mm. The defocusing distance, which refers to the distance of the beam waist (focal spot) from the top surface of the work-piece, is positive above, and negative below, the top surface. Other parameters such as fiber and focusing optics conditions were fixed at fiber diameter of 0.6 mm, collimation lens of 200 mm, focusing lens of 150 mm, and focusing spot diameter of 0.45 mm. Inconel 718 filler wire with a nominal diameter of 0.89 mm (0.035″) was used at an angle of 30° with the work-piece surface and wire feed rate of 4.5 m/min. The feed rate of the filler wire was calculated by using the volume flow rate constancy principle. For each pre-weld heat treatment condition, 3 butt joints were prepared: 2 for post-weld heat treatments (i.e., aged, or solution treated and aged) and 1 for as-welded condition (Table 2). The specimens were solution heat treated at 993 °C for 1 h and then argon quenched while the aging process of the weld joints was carried out as described above. The post-weld solution treatment was considered as a possible alternative to overcome the problems associated with niobium segregation and the formation of Laves phase [7]. However, this consideration has practically restricted the solution treatment temperature to approximately 995 °C, which is the solvus temperature of the orthorhombic Ni_3Nb delta phase (the precipitation temperature for delta phase ranges from 860 to 995 °C), to avoid undesirable grain coarsening at higher solution temperatures [8].

Table 2 Pre- and post-weld heat treatments for 3.18-mm Inconel 718 sheets

Specimen ID	Pre-weld heat treatment	Post-weld heat treatment
IN80	Solution treated (STed)	As-welded
IN81	Solution treated (STed)	Aged
IN75	Solution treated (STed)	STAed
IN78	Solution treated and Aged (STAed)	As-welded
IN82-2	Solution treated and Aged (STAed)	Aged
IN82-1	Solution treated and Aged (STAed)	STAed

Each weld joint was sectioned transverse to the welding direction using a precision cut-off saw to extract two specimens for metallographic examination. The remaining parts of the joints were used for tensile testing. Approximately 15–25 mm was cut from both sides of each joint to avoid edge effects and unstable welding conditions occurring at the start and the end. After cutting, each specimen was hot mounted in conductive Bakelite (Struers LaboPress-3), ground, and polished. Electrolytic etching was usually used, and two different etchants were employed to reveal the microstructure, depending on heat treatment conditions. Specimens were immersed in a solution of 25 g chromium trioxide (CrO_3) with 130 mL acetic acid (50%) and 7 mL distilled water. A voltage of 3.5 V was applied for 30 s with the etching time depending on the sheet thickness and conductive Bakelite. For the two post-weld heat treatments (i.e., aged or STAed), the etchant mentioned above was not suitable to reveal the microstructure of Inconel 718 alloy and thus a new etchant was applied. The specimens were immersed for a few seconds in a solution composed of 95 mL HCl plus 5 mL H_2O_2 for metallographic analysis. An optical microscope (Olympus GX-71) coupled with image analysis software (Analysis Five) was used to study weld geometry and to characterize the microstructure. Microstructure was also observed using a Hitachi S-3600N SEM with EDAX Genesis EDS system. For each sample, weld width (top, middle, and bottom), fusion-zone area, and discontinuities such as porosity, underfill, and weld reinforcement, if any, were measured. Vickers hardness was measured on each specimen at a testing load of 500 g, a dwell time of 15 s, and an indentation spacing of 0.2 mm using a Struers Duramin A300 Vickers microhardness machine. The hardness was usually measured along the middle-thickness of the joint.

For each weld specimen, four subsize tensile specimens were machined according to ASTM E8M-01, to give gauge dimensions of 6.0-mm width, 32-mm parallel length, and 125-mm overall length. The tensile specimens were tested at room temperature using a 50 kN Instron machine (model 1362) with self-locking grips and type 2620-604 Instron extensometer (a gage length of 25 mm used). The cross-head speed was fixed at 2 mm/min. For each tensile test, the data were converted from load and displacement to stress and strain, respectively, in order to obtain the stress–strain curve and to calculate yield strength at 0.2% offset, tensile strength, and plastic elongation percentage.

Results and discussion

Geometries

Figure 1 shows the transverse sections of all joints. The effect of post-weld heat treatment on joint dimensions appears to be insignificant and thus the measured joint dimensions are presented according to the pre-weld heat treatment conditions (Table 3). No significant differences in joint geometries were observed for the two pre-weld heat treatment conditions indicating that similar energy absorptivity of the laser beam is obtained for the STed, or the STAed conditions. In other words, the aging treatment of Inconel 718 alloy has little influence on the energy absorptivity of the laser beam.

Defects

As shown in Table 3 and Fig. 1, some minor underfill defects were observed. Sound joints were obtained, but some porosity was found in the fusion zone in some specimens. Figure 2 shows some microporosity obtained in the STed/as-welded condition. Figure 3 shows some porosity observed in the STAed/aged condition. Figure 4 shows some microporosity obtained in the STAed/as-welded condition. As shown in Table 3 and Fig. 1, slightly more porosity is observed when the material was welded in the STAed condition. Most of the pores have dimensions less than 0.1 mm and their number is quite low. However, large porosity can occasionally be observed as shown in Fig. 3.

In the fusion zone, neither macrocracks nor microcracks were observed. However, liquation microfissures are frequently observed in the HAZ as shown in Fig. 5. Figure 6 shows the SEM observations obtained in the STed/as-welded condition. It was reported that microfissures can be avoided using a low power pulsing wave Nd:YAG laser [4, 7, 10] and high power CO_2 laser [5]. Therefore, HAZ cracking is still an issue in high power Nd:YAG laser welding for Inconel 718 alloy. The liquation cracks usually occur normal to the fusion line and along the grain boundaries in the HAZ. The backfilling of cracks near the fusion zone was observed, as shown in Fig. 6. They are mainly observed beneath the "nail head" region of the laser welds, similar to those in electron beam welds [12]. As shown in Fig. 7, the composition of the grain boundary

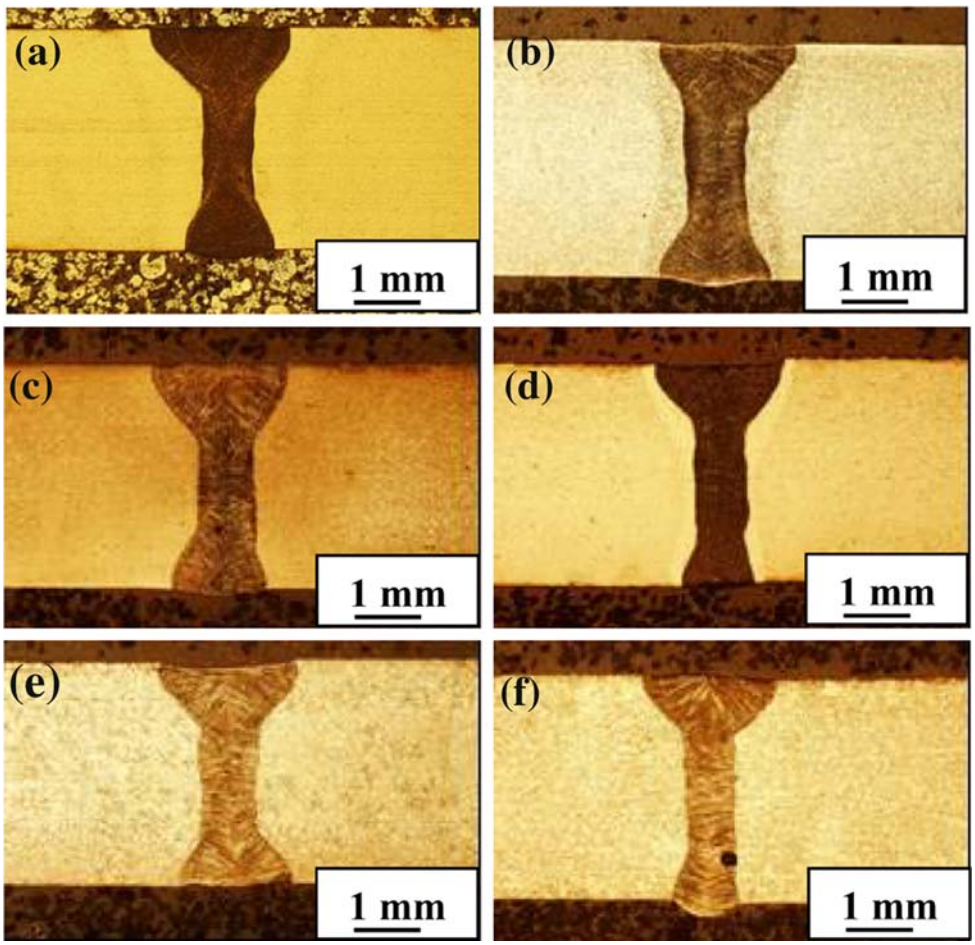

Fig. 1 Transverse sections of all butt joints. Heat treatment conditions are indicated as prior to/after welding (*STed* Solution Treated, *STAed* Solution Treated and Aged). **a** STed/As-welded. **b** STAed/As-welded. **c** STed/Aged. **d** STAed/Aged. **e** STed/STAed. **f** STAed/STAed

Table 3 Joint geometries and defects

	STed prior to welding		STAed prior to welding	
	Average	STDEV	Average	STDEV
Top width (mm)	2.06	0.15	1.91	0.11
Middle width (mm)	0.78	0.05	0.79	0.07
Root width (mm)	1.29	0.25	1.20	0.41
Fusion zone area (mm^2)	3.78	0.16	3.53	0.37
Top underfill area (mm^2)	0.05	0.06	0.08	0.10
Crown height (mm)	0.01	0.04	0.02	0.02
Crown area (mm^2)	0.01	0.04	0.01	0.01
Root underfill area (mm^2)	0.00	0.01	0.01	0.03
Root height (mm)	0.14	0.09	0.11	0.07
Root area (mm^2)	0.10	0.06	0.16	0.22
Fusion zone porosity (mm^2)	0.00	0.00	0.02	0.03

STDEV STandard DEViation

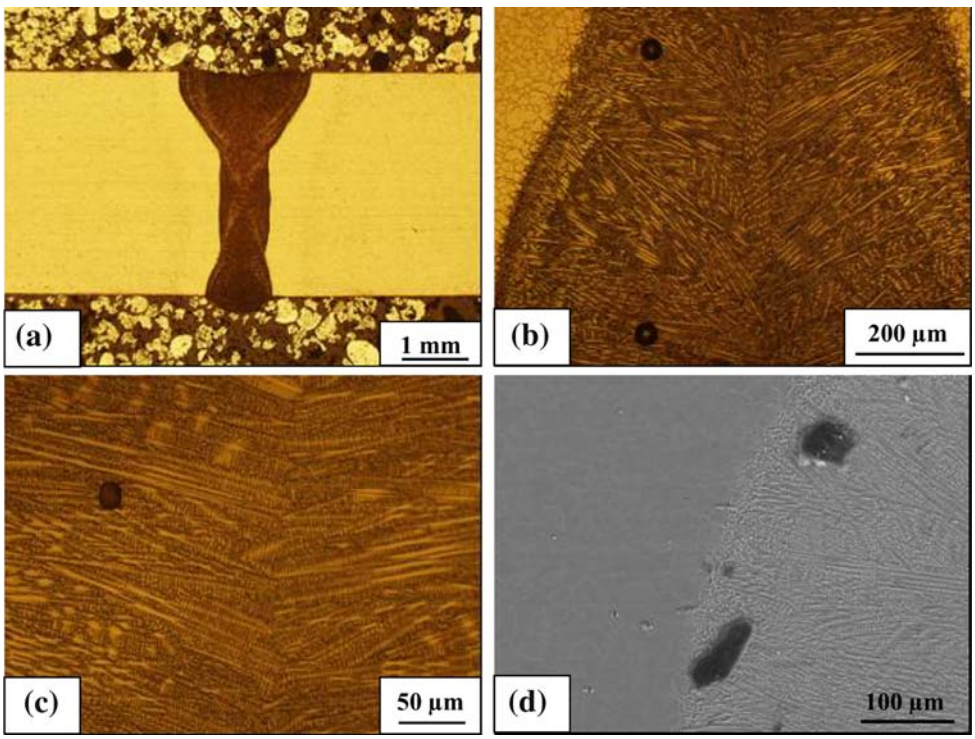

Fig. 2 **a** Overview of the weld joint obtained at STed/As-welded condition, **b**, **c** Microporosity in the fusion zone obtained in (**a**) and **d** microporosity obtained in another section of the specimen

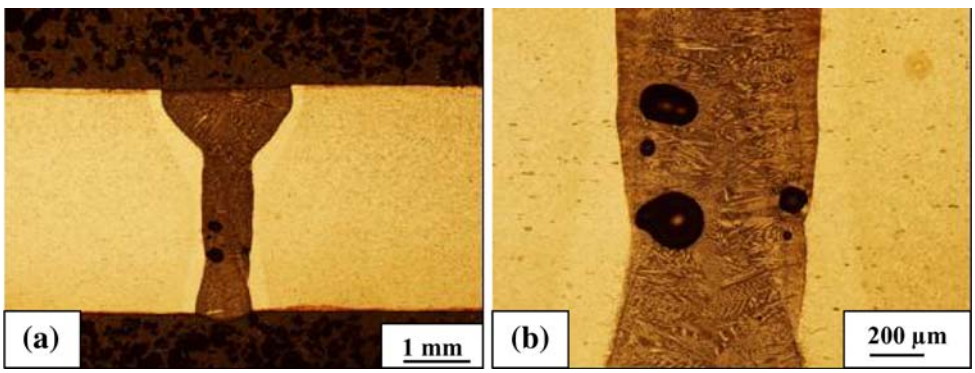

Fig. 3 **a** Overview of specimen obtained at STAed/Aged condition and **b** porosity in the fusion zone

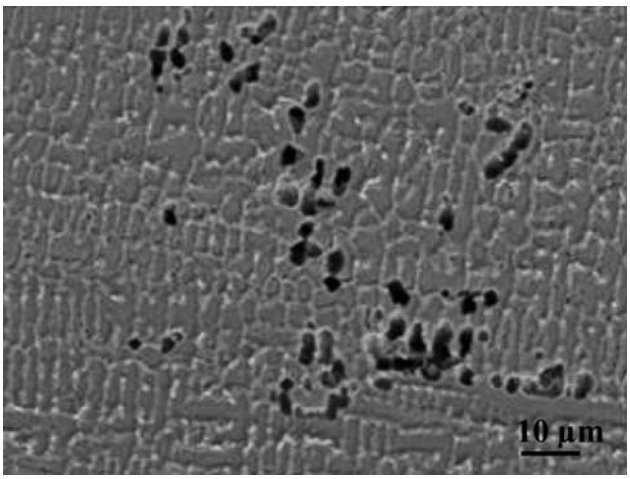

Fig. 4 Microporosity in the fusion zone obtained at STAed/As-welded condition

constituents is compared with that of the adjacent grain interior in the HAZ indicating that the grain boundary constituents have a noticeable higher Nb content. Therefore, the HAZ grain boundary cracking/separation could be associated with Nb-rich constituents in the grain boundary in agreement with the reported data relating the HAZ microfissuring to the constitutional liquation of NbC particles in HAZ grain boundaries [12]. Thompson et al. [13] also suggested that the segregation of the element S at the grain boundary is responsible for HAZ cracking in Inconel 718 alloy. It was also reported that the segregation of the element B, a melting point depressant of Ni, at grain boundaries is a major cause of liquation cracking in Inconel 718 alloy [14]. After the weld joints are solution treated and aged, much less grain boundary liquation cracking is observed (Fig. 5e, f). The mechanism remains to be mysterious. Further work is needed to clarify this in the future.

Previous investigations have shown that, the HAZ microfissuring tends to be enhanced by welding in the aged condition; coarse-grain size; presence of Laves phase; excessive amounts of NbC and delta phases at the grain boundary; higher amounts of boron in the base metal; sharp sectional variations in weld shape as in nail-head shaped welds; and other welding conditions which may promote high solidification stresses [7, 8]. As shown in Fig. 5a–d, no significant difference in the HAZ microfissuring is found in the pre-weld STed, or STAed conditions.

Centerline grain boundary was frequently observed as shown in Fig. 8. It is usually visible from the top surface along the entire joint thickness. Centerline grain boundary should be avoided because it may constitute a potential weldability issue [15, 16]. A centerline grain boundary represents a potentially harmful defect in a weld since it is the last region of the weld to solidify and thus is usually enriched in alloying elements and impurities. Therefore, centerline grain boundary may contain (i) low melting point constituents, making them potentially subject to incipient melting during heat treatment or service; (ii) eutectic and brittle phases, causing lower mechanical or corrosion resistance than the base material; and (iii) low toughness compared with other grain boundaries in a weldment, making crack propagation along them easier, and potentially harmful owing to their regular nature. In some circumstances, the formation of centerline grain boundaries may be related to the occurrence of solidification cracking due to low ductility and positive transverse stress [15, 16]. Centerline grain boundary is usually formed at high welding speeds, as typically experienced in laser welding. In this case, the weld pool usually has an arrow headed trailing edge or tear-shape and/or is concave [3]. This is due to both the elongation of the temperature field and the increase of growth undercooling with welding speed. The dendrites growing from both sides meet along the centerline of the weld, forming a planar centerline grain boundary [15]. This is a weak plane associated with the high tensile stress caused by the welding and solidification process, which leads to cracking along the weld centerline [3]. In Inconel 718 alloy, the centerline grain boundaries and the interdendritic areas may contain some Nb-rich Laves phases due to the segregation of niobium, which accumulates at the front of liquid–solid interface [4, 7, 8, 17, 18]. The Laves phase morphologies have been reported to be related to dendrites morphologies [7, 8]. In addition, the Laves phase can be interconnected, which is known to be more detrimental to tensile properties than fine Laves particles. To avoid the centerline grain boundary, the weld pool should have an elliptical or rounded shape and be convex. The solidifying grains are more randomly dispersed and do not meet at the center of the weld in a straight line, thus making centerline cracking much less likely [3].

Microstructures

The as-received (solution treated) microstructure of the base material consisted of equiaxed austenitic grains (Fig. 9a). The γ grains are a face-centered-cubic (fcc) nickel base austenitic continuous phase with solid solution elements such as Co, Cr, Mo, and W. Randomly distributed Nb-rich MC type primary carbides and carbonitrides were also observed. In addition, some needle-like δ phase can also observed, as typically shown in Fig. 9b. The grain size was measured manually using a lineal intercept method according to ASTM E112. For statistically representative results, 1,900–2,000 grains were sampled. Average grain sizes of 15.0 μm (ASTM 8.5–9.0) with standard deviation of 1.7 were obtained for the 3.18-mm base metal sheets in the solution treated condition. Pre- and post-weld aging

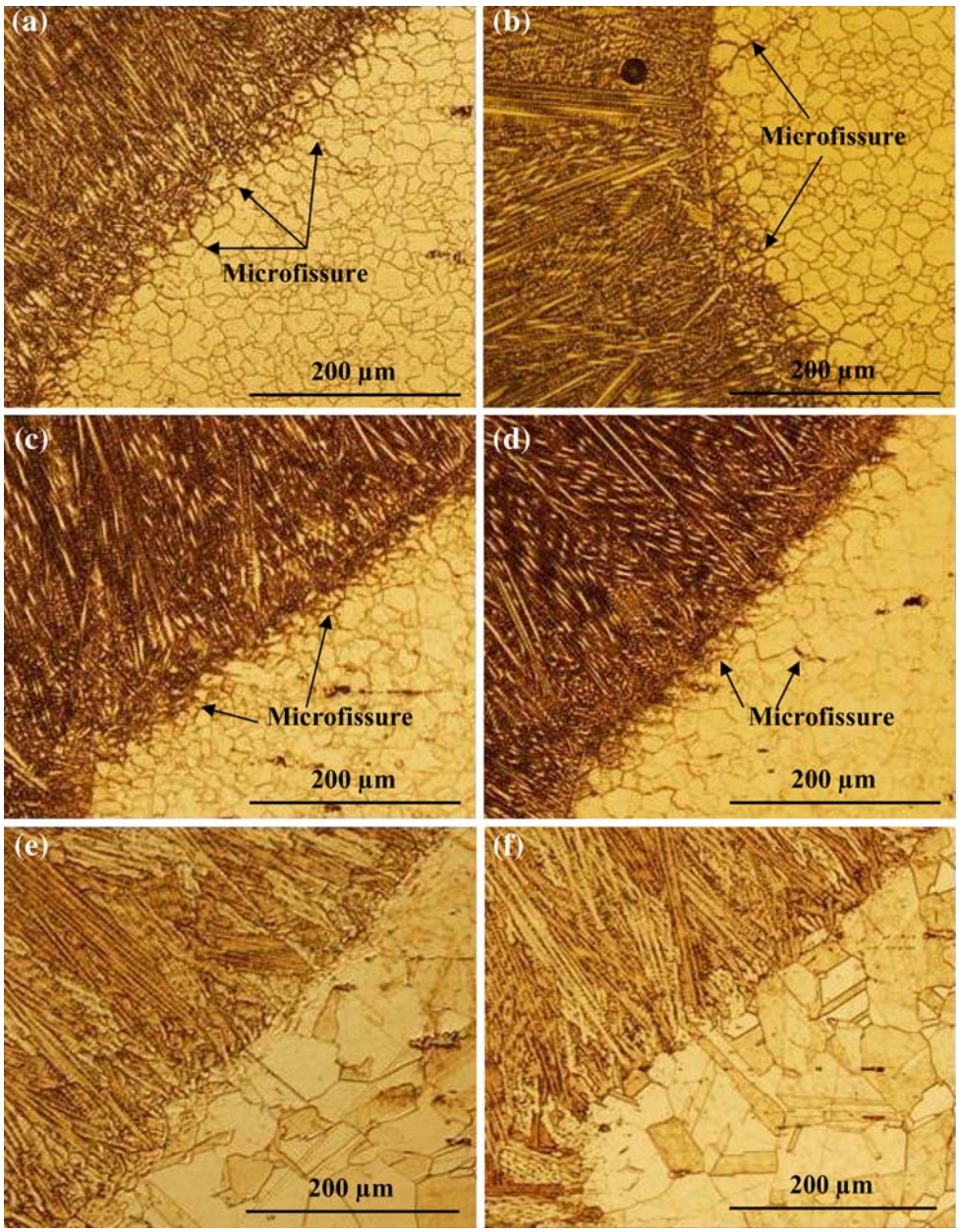

Fig. 5 Microfissures in the HAZ. **a** STed/As-welded, **b** STAed/As-welded, **c** STed/Aged, **d** STAed/Aged, **e** STed/STAed, and **f** STAed/STAed

treatment did not result in any perceivable change in the base metal microstructure and thus have insignificant influence on the grain size. For example, the average grain size in the STAed/as-welded condition is approximately 16.7 µm (standard deviation of 1.4), corresponding to ASTM grain size number of 9. Certainly the aging treatment can cause precipitation of the strengthening phases, but they cannot be observed using optical and SEM due to their extremely small size. However, post-weld solution treatment and aging results in considerable grain coarsening in the base metal, as shown in Fig. 9c, d. An average grain size of 44.6 µm with standard deviation of 4.7 (ASTM grain size number of 5.5–6) was obtained in the STAed/STAed condition. Clearly, significant grain coarsening appears in the post-weld solution treatment, i.e., the base metal was solution treated for a doubled holding time (2 h) compared with the base material in the as-received (STed) condition.

The effect of pre- and post-weld heat-treatment on the fusion zone microstructure is shown in Fig. 10. Typically, elongated dendrites were obtained. Alloy 718, being a heavily alloyed material, solidifies in a dendritic mode. The dendrites extend from the fusion zone boundary to the weld center. In laser welding, rapid cooling rate leads to very fine dendritic structures in the fusion zone. As shown in optical micrographs (Fig. 10), Laves and other hard phases in interdendrtic regions become dark after etching compared with the dendritic cores. However, Laves phase

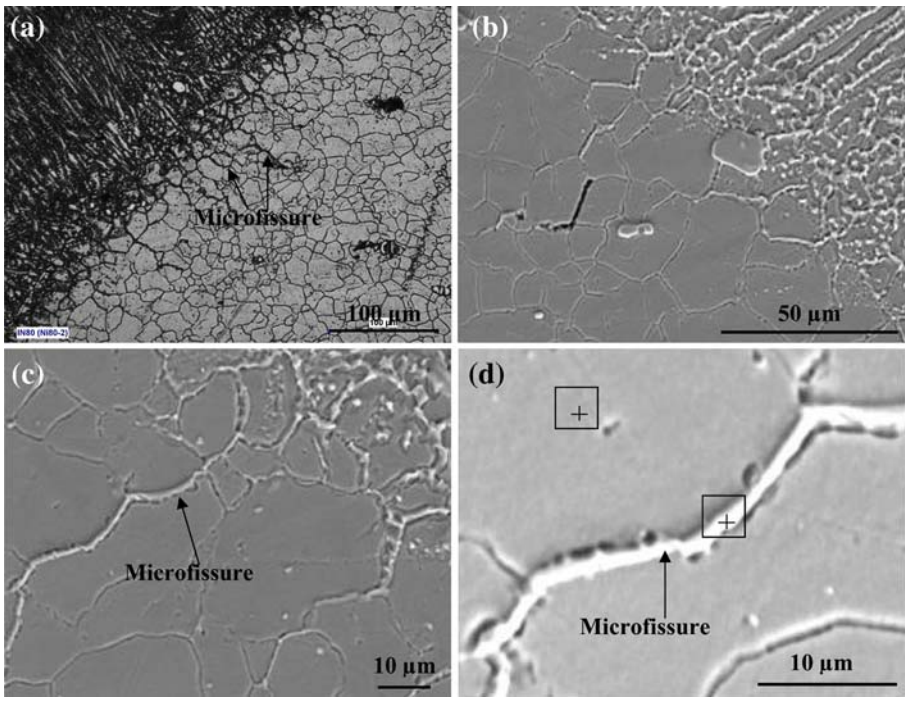

Fig. 6 HAZ liquidation cracking obtained at STed/As-welded condition

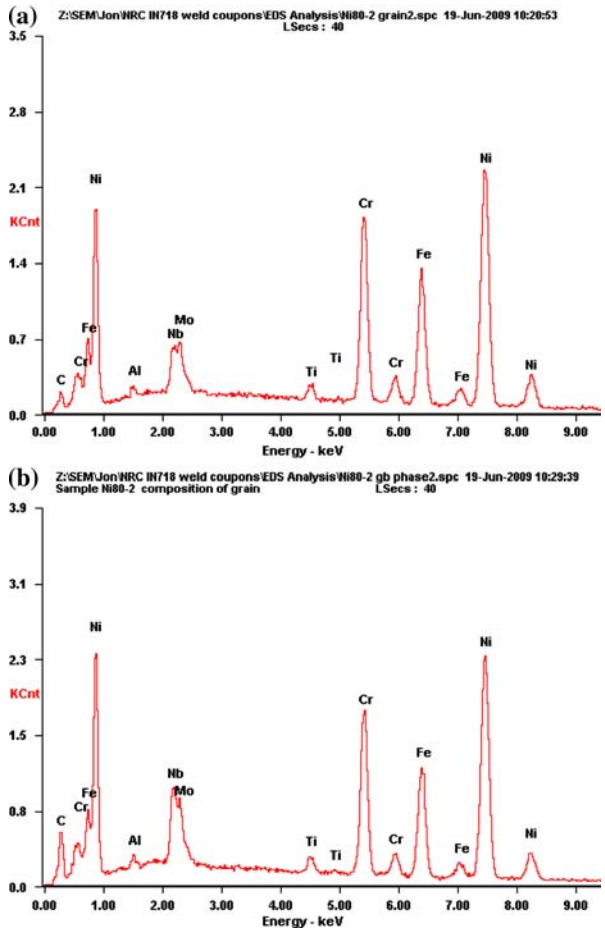

Fig. 7 SEM energy dispersive microanalysis of **a** matrix and **b** grain boundary indicated in Fig. 6d obtained at STed/As-welded condition

appeared to be white in SEM secondary images as shown in Fig. 11 because of higher emission of electrons from Laves phase [19]. In laser welding, the rapid cooling rate can also extend solute solubility which prevents marked segregation and the formation of a large eutectic. During solidification, the elements Nb, Ti, and Mo accumulate at the front of the liquid/solid interface and segregate to interdendritic areas where carbide (NbC, fcc) and Laves (Ni_3Nb, hexagonal $MgZn_2$ type) may form [10]. The gamma + NbC eutectic is suppressed during rapid cooling [10]. As shown in Fig. 11, the interdendritic Nb-rich Laves phase, whose morphologies are related to the dendrites structure, may form an interconnected network [7, 8]. Studies have shown that the formation of the Laves phase (i) depletes principal alloying elements required for hardening from the matrix, (ii) represents a weaker fusion zone microstructure between the Laves phase and the matrix interface by segregation of useful strengthening alloying elements, and (iii) act as preferential sites for easy crack initiation and propagation. The inherent brittle nature of the Laves phase leads to poor tensile ductility, fracture toughness, fatigue, and creep rupture properties in 718 alloy welds and castings [7–9, 20]. Therefore, the Laves phase is detrimental and hence should be carefully controlled. Compared with the as-welded conditions, less Laves particles are observed in the interdendritic regions after post-weld solution and aging treatment. Thus, the post-weld solution treatment at 993 °C resulted in considerable dissolution of the Laves particles. In this case, less interdendritic constituents were observed, as shown in

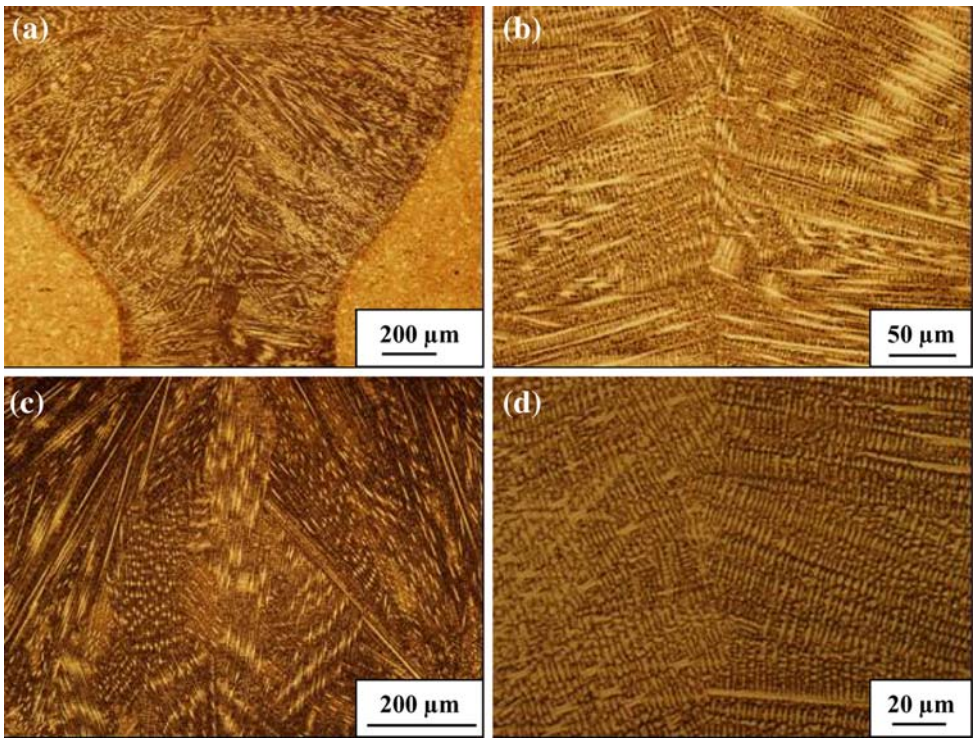

Fig. 8 Centerline grain boundary obtained at STed/Aged condition

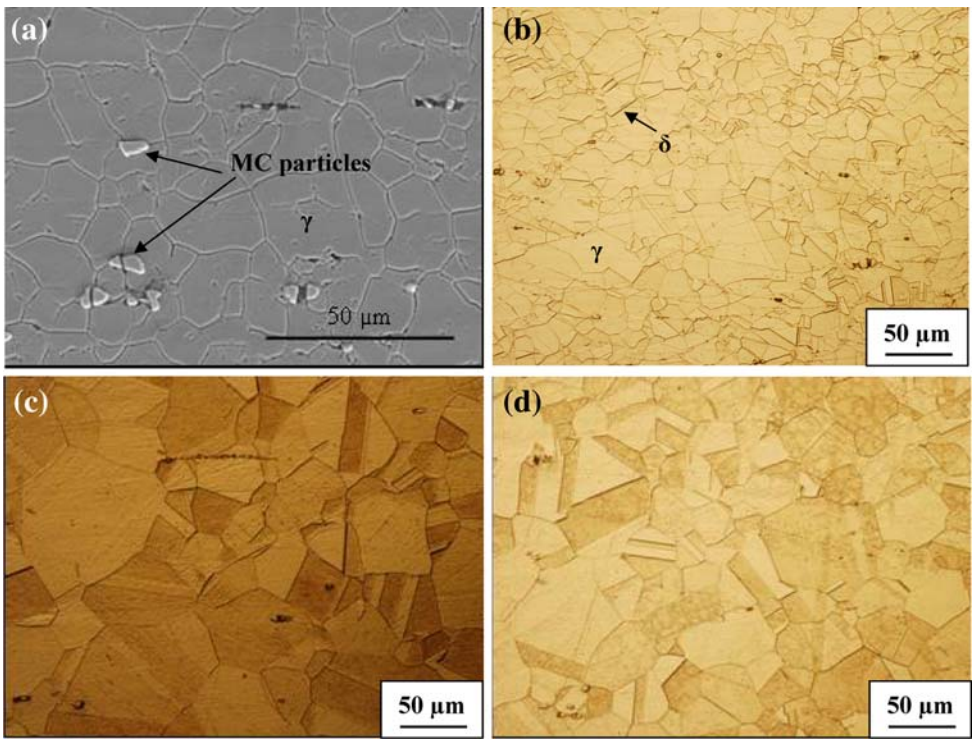

Fig. 9 Microstructures of base metal. **a** STed/As-welded, **b** STAed/As-welded, **c** STed/STAed, and **d** STAed/STAed

Fig. 12b. The initial solutionizing temperature of Laves phase is about 1,010 °C. Thus temperature of post-welding solution treatment should be higher than 1,000 °C to completely dissolve the Laves phase [10]. However, the improved dissolution characteristics of Laves phase in laser welds as obtained at lower temperature (993 °C) result from its fine, relatively discrete particle morphology, and low Nb concentration [7].

Solidification in Inconel 718 alloy starts with the primary liquid → γ reaction, causing the enrichment of Nb, Mo, Ti, and C in interdendritic liquid. The subsequent liquid → (γ + NbC) eutectic reaction consumes most of

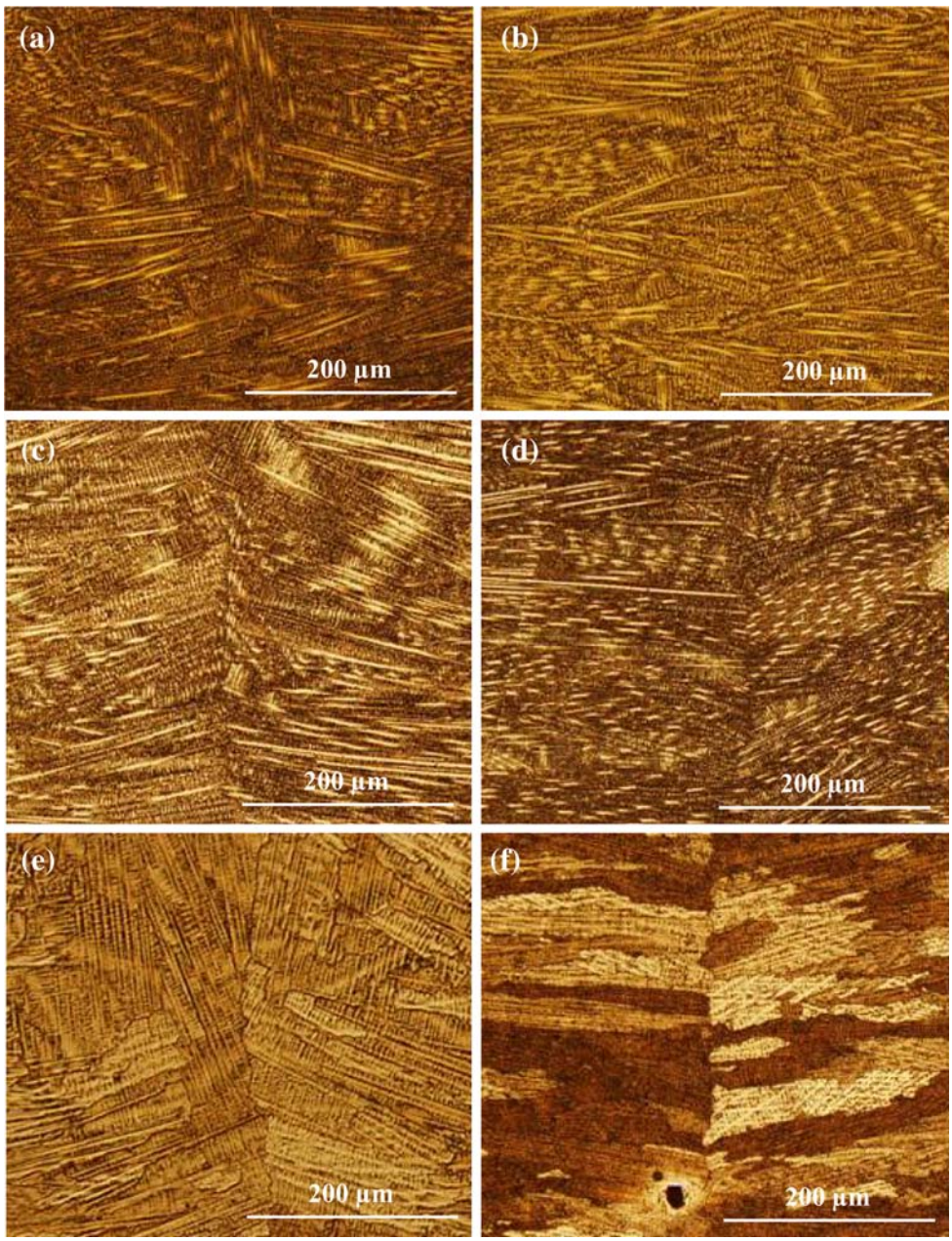

Fig. 10 Microstructures of the fusion zone. **a** STed/As-welded, **b** STAed/As-welded, **c** STed/Aged, **d** STAed/Aged, **e** STed/STAed, and **f** STAed/STAed

carbon available in the material until another eutectic type reaction liquid $\rightarrow (\gamma + \text{Laves})$ occurs, terminating the solidification process [7, 8]. The detrimental Laves phase is an unavoidable terminal solidification phase in Inconel 718 alloy. However, solidification conditions can strongly influence the extent of niobium segregation and hence the amount of Laves phase. The Laves particles are usually rich in Nb, Ti, Mo, Si, and lean in Fe, Cr, and Ni compared to the base metal [7]. Both the amount of Laves phase and Nb segregation are a function of solidification conditions. Compared with conventional arc welding processes, the extremely high cooling rate experienced in laser welding results in a much lesser extent of Nb segregation because of the insufficient time for solute redistribution. Hence, fewer Laves particles and a lower Nb concentration in Laves are obtained [8].

Compared with the base metal microstructure with the same pre- and post-weld heat treatment, similar microstructures are also observed in the HAZ (Figs. 5, 9). The HAZ was observed to be extremely narrow with no significant grain growth.

Mechanical properties

The Vickers microindentation hardness was performed for each welding condition along the middle-thickness.

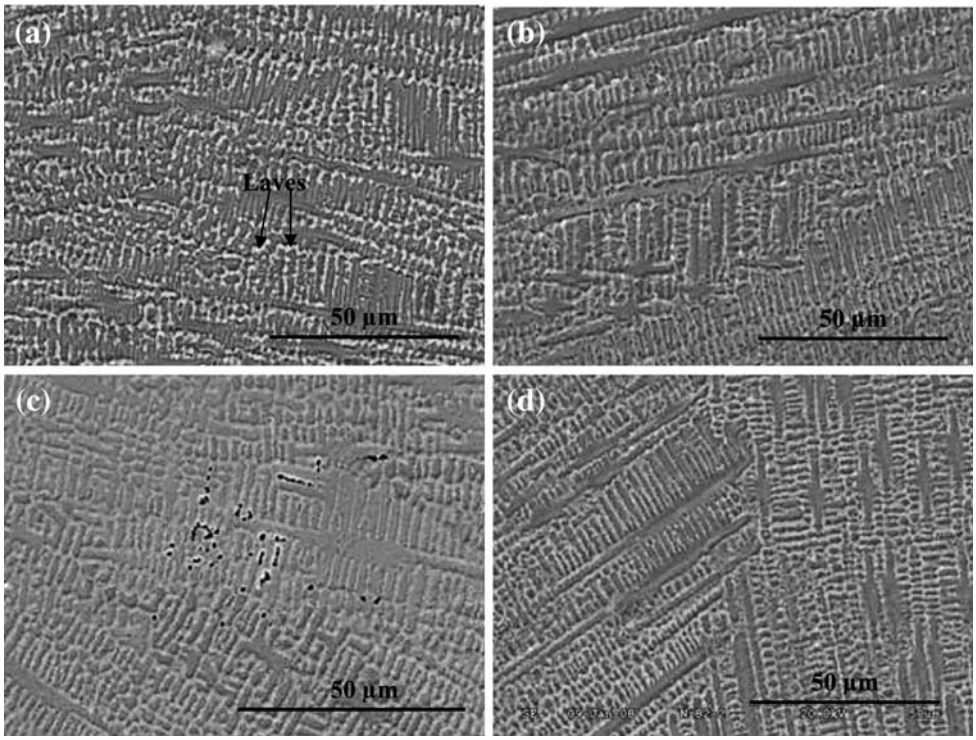

Fig. 11 SEM secondary electron images indicating the microstructures of the fusion zone. **a** STed/As-welded, **b** STAed/As-welded, **c** STed/Aged, and **d** STAed/Aged

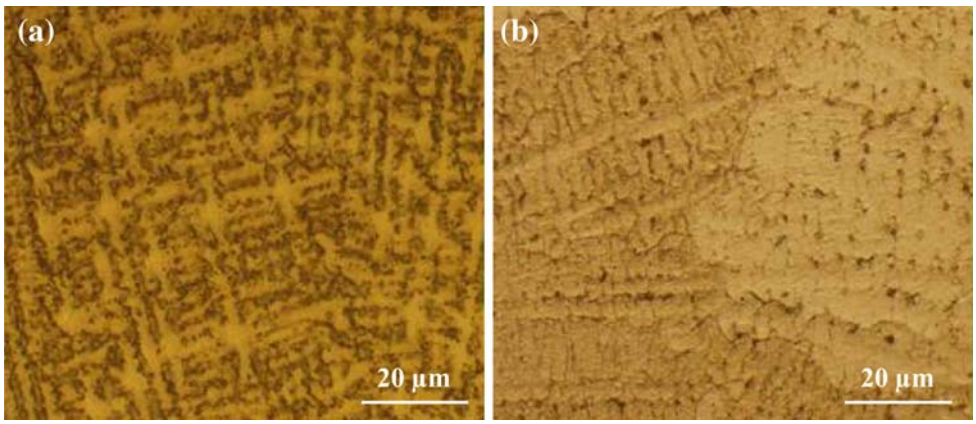

Fig. 12 Optical micrographs indicating the microstructure in the fusion zone. **a** STAed/As-welded and **b** STed/STAed

Typical hardness profiles across the welds are shown in Fig. 13 and the average values are given in Table 4. The base metal has an average value of approximately 221 HV in the solution treated condition. The aging treatment or the full heat treatment (solution treated and aged) either prior to or after welding can double the hardness values of the base metal (see Table 4).

If welded in the as-received condition (solution treated), the highest hardness is achieved in the fusion zone, which is probably due to the refined grain structure (Fig. 13a). For the material welded in the fully heat treated condition (solution treated and aged), however, the fusion zone hardness in the as-welded condition drops by half compared to that of the base material (Fig. 13b). The weld heat cycle occurring during laser welding may dissolve the principal strengthening phase γ'', whose dissolution temperature is around 900 °C. However, the fusion zone hardness is still higher than that in the solution treated base metal, probably due to the refined grain structure. The HAZ hardness was found to decrease significantly from the boundary between the base metal and the HAZ to the fusion line. The HAZ width is approximately 0.7 mm on each side of the fusion zone. The narrow HAZ is due to the low heat input and localized heating in laser welding. The softening of the metal in the HAZ is due to annealing [21].

As shown in Fig. 13c, d, the fusion zone has similar hardness to that of the fully heat treated base metal after post-weld aging. These increases in the fusion zone hardness are related to the re-precipitation of γ''. The full heat treatment (solution treatment and aging) after welding can

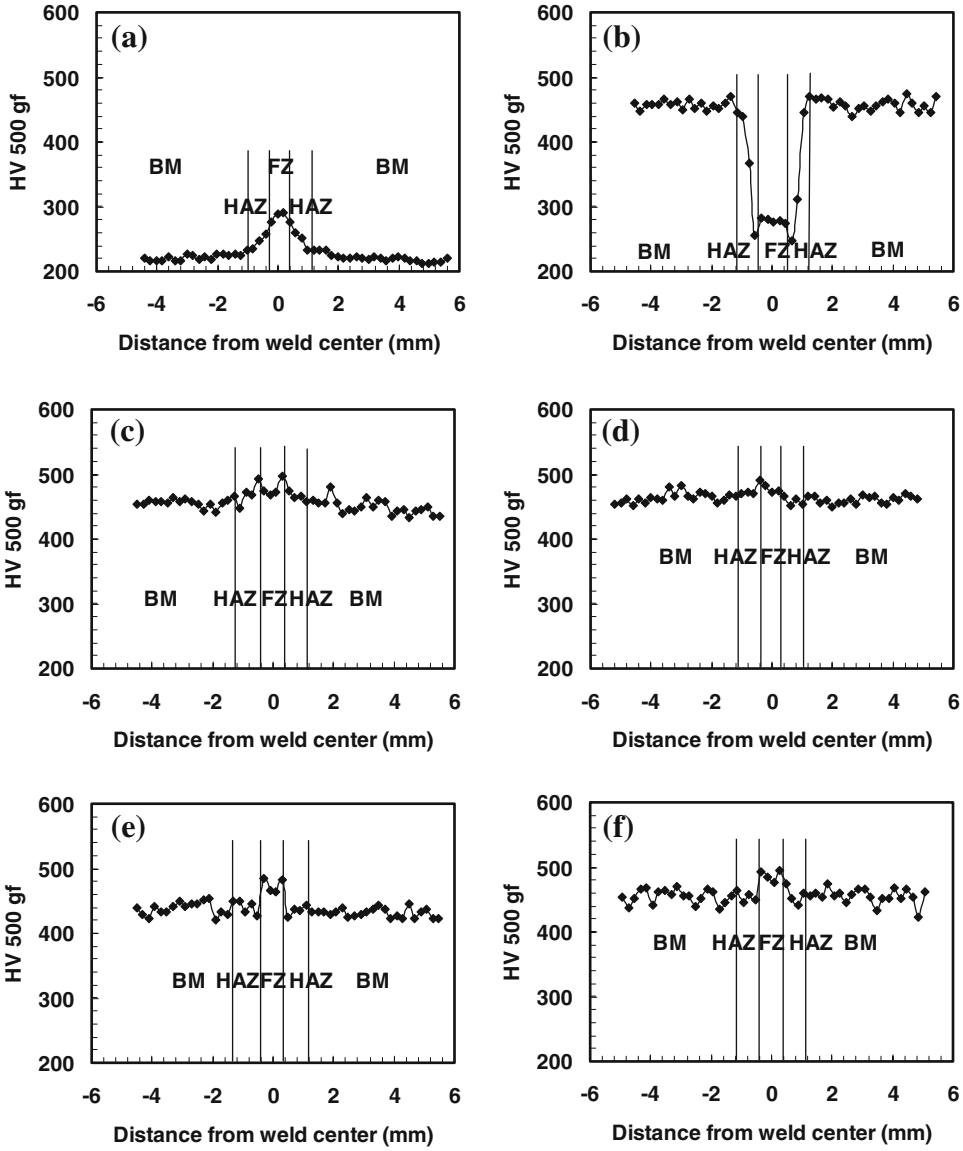

Fig. 13 Effect of pre- and post-weld heat treatment on hardness distribution. **a** STed/As-welded, **b** STAed/As-welded, **c** STed/Aged, **d** STAed/Aged, **e** STed/STAed, and **f** STAed/STAed

Table 4 Average hardness values

Pre-/post-weld heat treatment	FZ	HAZ	BM
STed/As-welded	287.6 ± 11.9	243.6 ± 27.5	221.1 ± 10.0
STed/Aged	483.1 ± 29.1	463.9 ± 23.8	450.7 ± 17.7
STed/STAed	489.2 ± 19.7	448.2 ± 16.8	445.3 ± 24.9
STAed/As-welded	277.5 ± 11.5	372.9 ± 186.3	459.3 ± 14.5
STAed/Aged	476.5 ± 23.4	463.2 ± 23.9	457.4 ± 15.1
STAed/STAed	489.7 ± 19.0	453.7 ± 20.1	455.3 ± 26.1

Note: Average value ± 2 Standard deviation

lead to slightly higher hardness in the fusion zone compared with that of the base metal. This slight improvement may be due to the greater dissolution of Laves phases in the fusion zone [7, 8]. Laves phase present in the weld microstructure consumes most of the Nb originally present in the base material, thereby making less Nb available for the precipitation of γ'', the principal strengthening phase. During post-weld solution treatment, the dissolution of Laves phases releases niobium. Thus, more Nb is available for γ'' precipitation and hence, niobium segregation may be reduced. This may increase the hardness in the fusion zone after the full post-weld heat-treatment compared with the post-weld aging treatment, in which the Laves phase remained as in the as-welded condition (Fig. 13c–f).

Table 5 Tensile properties

Pre-/post-weld heat treatment	YS (MPa)	TS (MPa)	El (%)
STed/As-welded	451.9 ± 5.2	897.2 ± 5.8	39.6 ± 1.6
STed/Aged	1177.2 ± 24.5	1401.3 ± 26.6	15.8 ± 14.4
STed/STAed	1075.8 ± 9.6	1318.2 ± 15.6	16.5 ± 1.8
STAed/As-welded	727.2 ± 23.8	1031.1 ± 20.6	2.9 ± 0.2
STAed/Aged	1188.7 ± 12.0	1402.7 ± 3.1	12.9 ± 1.2
STAed/STAed	1079.18 ± 7.2	1314.2 ± 9.9	20.4 ± 2.8

Note: Average value ± 2 Standard deviation

Precipitation of these phases in weld metal cannot take place during welding due to the very rapid thermal cycle, thus necessitating post-weld aging treatment [8].

The tensile specimens used for the base metal (Table 1) and the weld joints (Table 5 and Fig. 14) are different in dimensions and thus ductility results are not compared here. The following observations are mainly concentrated on yield and tensile strengths:

(i) If welded in the solution treated condition, the weld joints in the as-welded condition have similar yield and tensile strengths to those for the base metal, i.e., 100% joint efficiency can be obtained.

(ii) If welded in the solution treated and aged condition, the yield and tensile strengths of the weld joints in the as-welded condition are reduced compared with those for the base metal (Approximately 74% joint efficiency is obtained).

(iii) Higher yield and tensile strengths in the as-welded joints are obtained when welded in the solution treated and aged conditions than in the solution heat treated conditions.

(iv) If welded in the solution treated condition, the post-weld aging treatment significantly increases the yield and tensile strengths. Approximately 160% joint efficiency was obtained. This is a usual treatment for Inconel 718 alloy, i.e., welded in the solution-annealed condition followed by conventional aging heat treatment, which combines stress relief with precipitation of the strengthening phase [21].

(v) If welded in the solution treated and aged condition, the post-weld aging treatment can recover the yield and tensile strengths to the levels of the base metal, i.e., 100% joint efficiency can be obtained after post-weld aging treatment only.

(vi) Compared with the as-welded condition, the post-weld aging or full heat treatment can significantly increase the yield and tensile strengths, particularly if welded in the solution treated condition.

(vii) If welded in the solution treated condition, the post-weld solution and aging treatment can significantly increase the yield and tensile strengths. Approximately 150% joint efficiency can be obtained.

(viii) If welded in the solution treated and aged condition, the post-weld solution and aging treatment can recover the yield and tensile strengths almost to the levels of the base metal, i.e., approximately 94% joint efficiency can be obtained.

(ix) Compared with post-weld aging treatment, the post-weld solution and aging treatment results in slight decreases in yield and tensile strengths. The lower strength in the STAed conditions than in the aged is probably due to the presence of more δ-phase needles which acted as stress raisers in static loading [19]. Post-weld aging treatment is enough to strengthen the weld joints. This is quite different from the results reported by Ram et al. [7]. They concluded that post-weld solution and aging treatment improved all tensile properties, including yield strength, tensile strength, and elongation, compared with post-weld aging treatment in pulsed wave laser welded Inconel 718 alloy. For reasons of weldability and mechanical properties, it is usually advised that (a) these materials should be welded in the solution treated state and (b) post-weld solution and aging treatments with precipitation hardening should be carried out [6]. In the repair welding process of Inconel 718 alloy, the precipitation-hardened superalloys must also undergo PWHT, i.e., solution heat treatment followed by aging after weld repair, to restore the mechanical properties [22]. However, the present work indicates that post-weld aging can lead to better tensile strength than the post-weld full heat treatment. Therefore, the post-weld solution treatment may be eliminated. The solution treatment at high temperature cannot only consume energy but also cause distortion. The aging treatment can also relieve welding residual stress, improve stress corrosion cracking and reduce weld distortion. In addition, no significant grain growth in the HAZ appears during aging.

(x) As shown in Fig. 14c, higher joint efficiencies can be obtained in pre-weld solution treated than fully heat treated conditions. Post-weld aging or full heat

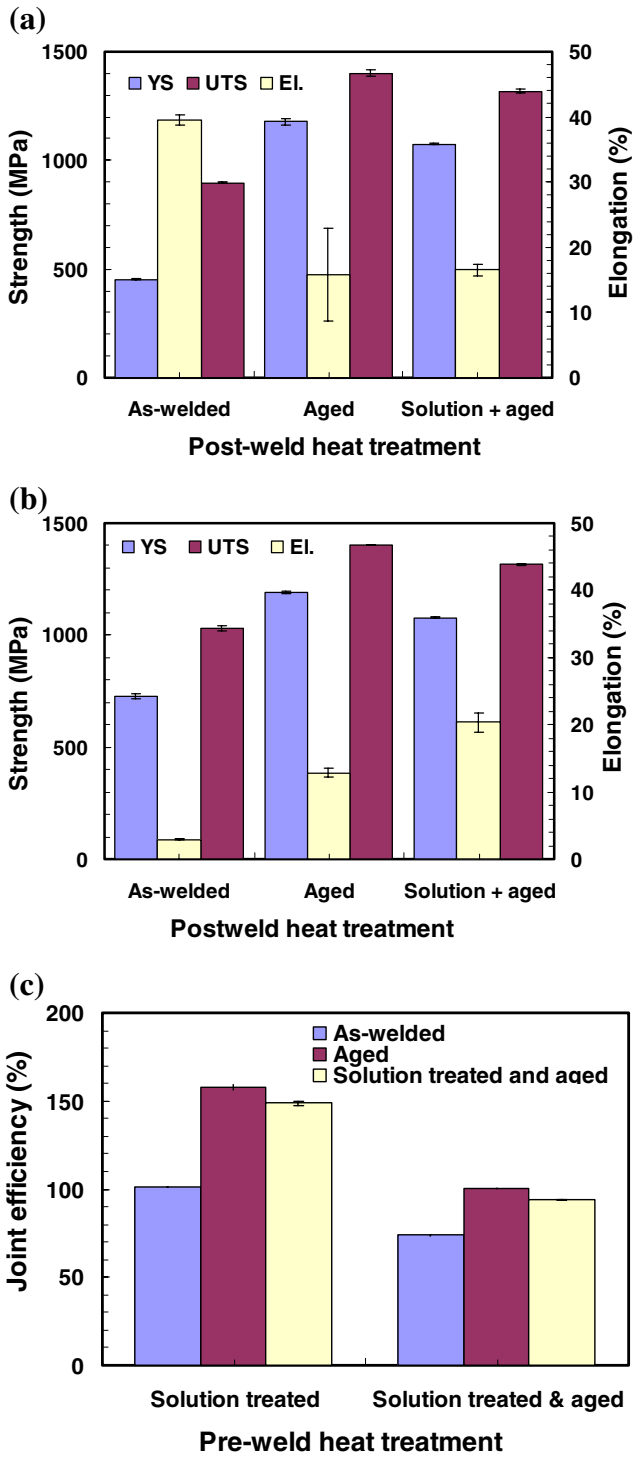

Fig. 14 Tensile properties: **a** solution heat treated prior to welding, **b** solution heat treated and aged prior to welding, and **c** joint efficiency

treatment can increase joint efficiencies. The highest joint efficiencies are obtained in post-weld aging condition.

During tensile failure tests, only one out of four tensile specimens in the solution treated/aged condition was fractured in the base metal. All other tensile specimens were fractured in the fusion zone indicating that the weld zone is the weakest location for the tensile failure. It has been reported that the interdendritic Laves phase in the weld fusion zone serves as microvoid nucleation sites [1]. The fracture occurred by microvoid coalescence, which was initiated by interdendritic constituents. This causes the fracture in the weld fusion zone and low ductility of the weld joints.

Inconel 718 alloy is usually not recommended to be welded in pre-weld full heat treatment condition [6, 12]. It was also reported that Inconel 718 alloy can be welded in both solution treated and fully heat treated states using 1 kW pulsing wave Nd:YAG and high power CO_2 lasers [4]. The present work indicated that Inconel 718 alloy can be welded using high power Nd:YAG laser in either pre-weld solution treated or fully heat treated conditions. For both pre-weld heat treatment states, no solidification cracking was observed in spite of the presence of HAZ cracking. Even so, pre-weld solution treatment is preferred. After welding, the aging treatment can be used to strengthen the welds.

Conclusions

1. Neither macrocracks nor microcracks are observed in the fusion zone. HAZ liquation cracking, however, is frequently observed in Inconel 718 alloy joints welded using high power Nd:YAG lasers. The liquation microfissures usually appear beneath the "nail head" region of the laser welds, normal to the fusion zone boundary, and along the grain boundaries in the HAZ.
2. Significant increases in the grain sizes of the welds are observed after solution treated and aged.
3. Higher yield and tensile strengths in the as-welded joints are obtained when welded in the solution treated and aged conditions than in the solution treated conditions prior to welding.
4. Compared with the as-welded condition, the post-weld aging treatment can significantly increase the yield and tensile strengths, particularly if welded in the solution treated condition. Compared with the post-welding aging treatment, the post-weld solution treatment and aging results in slight reduction in yield and tensile strength. In other words, only post-weld aging treatment is enough to strengthen the weld joints. The solution treatment at high temperature cannot only consume energy but also cause distortion. Therefore, post-weld solution treatment is not necessary for strength recovery.

Acknowledgements This report is part of the collaborative research Project between IAR-AMTC and SAL (46M3-J017). Thanks are due to E. Poirier and M. Banu, Technical Officers, for the preparation of weld joints, technical support to welding metallurgy, and tensile testing.

References

1. Hirose A, Sakata K, Kobayashi KF (1998) Int J Mater Prod Technol 13(1–2):28
2. Ping DH, Gu YE, Cui CY, Harada H (2007) Mater Sci Eng A 456:99
3. Tillack DJ (2007) Weld J 1:28
4. Gobbi S, Zhang L, Norris J, Richter KH, Loreau JH (1996) J Mater Process Technol 56:333
5. Fontana G, Gobbi S, Rivela C, Zhang L (1999) Weld Int 13(8):631
6. Cornu D, Gouhier D, Richard I, Bobin V, Boudot C, Gaudin JP, Andrzejewski H, Grevey D, Portrat J (1995) Weld Int 9(10):802
7. Ram GDJ, Reddy AV, Rao KP, Reddy GM, Sundar JKS (2005) J Mater Process Technol 167(1):73
8. Ram GDJ, Reddy AV, Rao KP, Reddy GM, Sundar JKS (2005) Mater Sci Technol 21(10):1132
9. Biswas S, Reddy GM, Mohandas T, Murthy CVS (2004) J Mater Sci 39:6813. doi:10.1023/B:JMSC.0000045609.86430.19
10. Li Z, Gobbi SL, Fontana G, Richter HK, Norris J (1996) Metall Ital 89:5041–5047
11. Cao X, Rivaux B, Jahazi M, Cuddy J, Birur A (2008) In: Jahazi M, Elboujdaini M, Patnaik P (eds) Aerospace materials and manufacturing: emerging materials, processes, and repair techniques, COM 2008: 47th conference of metallurgists, Winnipeg, Canada, August, 2008, pp 313–323
12. Lingenfelter A (1989) In: Loria EA (ed) Superalloy 718—metallurgy and applications. TMS, Warrendale, PA, pp 673–683
13. Thompson RG, Dobbs JR, Mayo DE (1986) Weld Res Suppl 11:299s
14. Chaturvedi MC (2007) Mater Sci Forum 546–549:1163
15. Hunziker O, Dye D, Reed RC (2000) Acta Mater 48:4149
16. Dye D, Hunziker O, Reed RC (2001) Acta Mater 49:683
17. Zhang L, Gobbi SL, Fontana G, Norris J, Richter HK (1997) Metall Ital 89(5):41
18. Ram GDJ, Reddy AV, Rao KP, Reddy GM (2004) Sci Technol Weld Joining 9(5):390
19. Sivaprasad K, Raman SGS (2008) Metall Mater Trans A 39A(9):2115
20. Radhakrishna CH, Rao KP (1997) J Mater Sci 32:1977. doi:10.1023/A:1018541915113
21. Yaman YM, Kushan MC (1998) J Mater Sci Lett 17:1231
22. Qian M, Lippold JC (2003) Mater Sci Eng A 340:225